Exploring the First Aerosol Indirect Effect over the Maritime Continent Using a Ten-Year Collocated MODIS, CALIOP, and Model Dataset

Alexa D. Ross[1], Robert E. Holz[1], Gregory Quinn[1], Jeffrey S. Reid[2], Peng Xian[2], F. Joseph Turk[3], Derek
J. Posselt[3]

[1]Cooperative Institute for Meteorological Satellite Studies, University of Wisconsin - Madison, Madison, WI, 53706, USA
[2]United States Naval Research Laboratory, Monterey, CA, 93943, USA
[3]Jet Propulsion Laboratory, Pasadena, CA, 91009, USA

Correspondence to: Alexa D. Ross (alexa.ross@ssec.wisc.edu)

5

10

15

20

1

Atmospheric
Chemistry
and Physics
Discussions

Abstract. Satellite observations and model simulations cannot, by themselves, give full insight into the complex relationships between aerosols and clouds. This is especially the case over the greater Southeast Asia, an area that is particularly sensitive to changes in precipitation yet possesses some of the world's largest observability and predictability

5   challenges. We present a new collocated dataset that combines satellite observations from Aqua's Moderate-resolution Imaging Spectroradiometer (MODIS) and the Cloud-Aerosol Lidar with Orthogonal Polarization (CALIOP) with the Navy Aerosol Analysis and Prediction System (NAAPS). The dataset is designed with the capability to investigate aerosol-cloud relationships and provides coincident and vertically resolved cloud and aerosol observations for a ten year period. Using model reanalysis aerosol fields from the NAAPS and coincident cloud liquid effective radius retrievals from MODIS

10   (removing cirrus contamination using CALIOP), we investigate the first aerosol indirect effect. We find overall that as expected, aerosol loading anti-correlates with cloud effective radius, with maximum sensitivity in cumulous mediocris clouds with heights in the 3-4.5 km level. The highest susceptibility in droplet effective radius to modeled perturbations in particle concentrations were found in the more remote regions of the western Pacific Ocean and Indian Ocean. Conversely, there was much less variability in cloud droplet size near emission sources over both land and water. We hypothesize this is

15   suggestive of a high background aerosol population already saturating the cloud condensation nuclei budget.

1 Introduction

The greater Southeast Asia (hereby SEA) has long been identified as an area of climate vulnerability (e.g. Cruz et al., 2007; Hijioka et al., 2013). As outlined in the review, Reid et al. (2013), the region has seen dramatic shifts in land use and anthropogenic emissions. While anthropogenic influences on the aerosol system are punctuated by dramatic deforestation

20   and biomass burning events in both the northern insular SEA of Myanmar, Thailand, Vietnam, Cambodia and Laos, and the Maritime Continent of Indonesia, Malaysia, Brunei and the Philippines, the region can also host pristine environments. Often thought of as remote, the population density in these regions can be exceptionally high, and the influence of industrial and domestic emissions is far reaching.

Large-scale climate change has manifested itself in temperature and rainfall signals (e.g., Cruz et al., 2013; Sharma and

25   Babel, 2014). A persistent question in the scientific community has been to what extent do aerosol emissions feedback onto meteorology and perhaps climate? Are aerosol particles a primary contributor to regional climate change, or do aerosol emissions have second or third order influences? There is evidence that severe storms in the region are enhanced by aerosol emissions (Yuan et al., 2011) and the range of aerosol conditions theoretically should lead to changes in cloud physics (e.g., Sorooshian et al., 2010; Rosenfeld et al., 2014). However, while a straightforward question with theoretical and some

30   observational backing, tracing aerosol influences from emissions to climate impact is difficult in any environment.

Addressing this question in Southeast Asia is particularly daunting; complex monsoonal flows, organized convection, and near ubiquitous cirrus challenge observations and models alike (Reid et al., 2013).

NASA sponsored an Interdisciplinary Science (IDS) grant to systematically examine the sensitivity rainfall in SEA has to aerosol particle effects. But given the complexity and poor observability of the Southeast Asian system, proper and testable hypotheses needed to be developed. A reasonable question was provided by Cruz et al. (2013) who found that there has been a steady increase in the number of "no rain days" in Philippine ground stations. The increase in no rain days occurs at the expense of "trace and light rain" days rather than moderate to heavy rainfall. Since it is trace or light rain events that appear to be largely affected, and such rain is often associated with precipitation from isolated warm convection that is thought to be more sensitive to increases in cloud condensation nuclei (CCN), perhaps this trend is associated with increasing aerosol loadings. Indeed, warm rain impacts have been repeatedly modeled (e.g., Langmann, 2007; Graf et al., 2009). However, aerosol particle lifecycle and regional meteorology are tightly coupled (e.g., Reid et al., 2012, 2015, 2016). Any study on SEA aerosol impact must then be wary of statistical confounding between aerosol and cloud phenomenon and any potential contextual, sampling, or measurement biases.

One approach to studying aerosol impacts in Southeast Asia is to make use of the NASA afternoon-train satellite orbit constellation (or A-Train). The A-train is anchored by Aqua's Moderate-resolution Imaging Spectroradiometer (MODIS) instrument, with significant synergy with other sensors such as aerosol and cloud profiling from the Cloud-Aerosol Lidar with Orthogonal Polarization (CALIOP) instrument on the Cloud-Aerosol Lidar and Infrared Pathfinder Satellite Observations (CALIPSO) spacecraft and the Cloud Profiling Radar (CPR) on the CloudSat spacecraft. Both MODIS and CALIOP instruments are sensitive to aerosol particles and clouds, but in regions with high cloud fraction such as SE Asia, there is often difficulty observing both cloud and aerosol particles in a column. MODIS collection 6 aerosol products, for example, have become quite clear sky conservative, yielding few retrievals in even moderately cloudy environments. Optically thin cirrus fraction in SEA complicates aerosol and low to mid-level cloud retrievals alike (Chew et al., 2011; Reid et al., 2013). Certainly, profiling instruments like CALIOP lack the ability to see aerosol particles below a cloud layer if the lidar's signal becomes completely attenuated from the cloud. CALIOP can only profile to an optical depth of approximately 3. Thus, even error propagation and boundary layer aerosol signals are problematic for penetration through optically thin clouds.

For the IDS project, one of the approaches was to develop an A-train "curtain product" for Southeast Asia where these satellite products were physically collocated and combined with modeled meteorology and aerosol data. The model can provide information on variability of aerosol properties through the atmospheric column, including estimates of aerosol type and source location based on back-trajectory analysis, providing information about the aerosol properties in the presence of cloud. CALIOP can provide context on cloud top height and the presence of thin cirrus, and MODIS provides aerosol and cloud retrievals. This combined product provides a unique suite of data to investigate aerosol-cloud-precipitation relationships with the needed information to control for environmental or observational confounding. This manuscript focuses on the relationship between aerosol amount and cloud droplet size using observations from MODIS and CALIOP.

Atmospheric
Chemistry
and Physics
Discussions

As a continuation of this research, subsequent manuscripts will include analysis using CloudSat observations to investigate aerosol-precipitation relationships. Due to a battery anomaly in 2011, CloudSat fell out of the A-Train orbit, so collocated CloudSat-MODIS-CALIOP observations only exist from 2006-2011. Thus, subsequent research investigating aerosol-precipitation relationships will be limited to a five-year time period. For the research presented in this manuscript, we

5   utilized the entire collocated MODIS-CALIOP record from 2006-2016.

The focus of this analysis is to investigate a cloud-aerosol relationship known as the first aerosol indirect effect (or FAIE), introduced by S. Twomey in 1974, with the premise that for aerosol particles to affect precipitation in isolated warm cumulus clouds, they likely have to first influence cloud effective radius (r_{eff}). Using the curtain dataset described herein, we first explore the observing challenges of the aerosol and warm convective cloud system, followed by an analysis that

10   includes the use of Navy Aerosol Analysis and Prediction System (or NAAPS; Lynch et al., 2016) reanalysis for aerosol detection. Indeed, model aerosol data has been combined with satellite retrieved properties before. Ma et al. (2010) uses aerosol concentrations simulated by the GOCART model to show a dependency of observed cloud droplet size – provided by MODIS – on organic carbon amounts. The study by Ma et al. (2010) was for a global domain and did not investigate the long-reaching effects of aerosol particles and the scale of the impact of pollution on cloud droplet size. Additionally, Ma et

15   al. (2010) did not investigate the dependency of the FAIE on cloud top height, which can be used as a proxy for filtering different types of cloud type meteorology.

This paper focuses on the MODIS, CALIOP and NAAPS components of the Southeast Asian Curtain Cloud-Aerosol Regional A-Train (CCARA) dataset, and structured in the following way. In Section 2, we describe the generation of the A-Train curtain dataset. In Section 3, we examine the baseline statistical properties and quality assurance of the products

20   therein, with a particular emphasis on sampling and the potential for thin cirrus cloud contamination. Section 4 provides results and discussions on observed relationships between aerosol and cloud r_{eff} properties. A final discussion and conclusion synopsis is provided in Section 5.

2 Methods: Development of the Southeast Asian Curtain Cloud-Aerosol Regional A-Train (CCARA) product

The dataset used here was developed specifically to meet the challenges of doing aerosol and cloud research in the complex

25   Southeast Asian environment. Here, we demonstrate this system at its simplest level as a launching point for more detailed analysis of the CCARA. The dataset is comprised of data from two satellite instruments and fields from two models. In short, the basis is the CALIOP footprint to provide cirrus screening and cloud height information. Other cloud properties are derived from MODIS. Aerosol properties are derived from the NAAPS-RA (which includes MODIS and MISR AOD data assimilation), with supporting meteorological information from the ECMWF reanalysis.

30   ### 2.1 Description of the satellite instruments

MODIS flies aboard the Aqua satellite, which launched in 2002 (Salomonson et al., 2002). The imager observes reflectance at 36 wavelengths in the visible and infrared bands and spatial resolutions ranging from 250 meters to 1 km. The MODIS products used in this research are from Level 2 Collection 6 (C6), provided at spatial resolutions spanning 1 to 10 km^2 at

nadir. In this study, the primary MODIS data used are cloud property products (MYD06; Platnick et al., 2017), the cloud mask products (MYD35; Ackerman et al., 1998) and aerosol product (MYD04, Levy et al., 2005). MODIS collocation indices are found using the MYD03 geolocation files at 1 km spatial resolution. ~~The collocation technique is discussed further in Section 2.3.1.~~ Partly cloudy (PCL) pixels are classified in the C6 MYD06 algorithm, but are not included in this

5   analysis.

The CALIOP instrument provides observations at two wavelengths: 532 nm (visible) and 1064 nm (near-infrared) with polarization capabilities in the 532-nm channel. The lidar has a vertical resolution of 30 m, producing detailed profiles of cloud and aerosol vertical structure. CALIOP Level 2 cloud products exist at horizontal resolutions of 333 meters, 1 km, and 5 km. CALIOP ~~Aerosol Level 2 products~~ exist at 5 km horizontal resolution. All of the CALIOP data used in this analysis

10   are from the 5-km cloud and aerosol products (CPRO and APRO) which while having 60 m vertical resolution, can include spatial averages up to 80 km depending on the ~~signal to noise~~ ratio. CALIOP Level 2 algorithms provide their own set of feature layers that can distinguish up to 10 cloud and aerosol layers (CLAY and ALAY; Winker et al., 2009). To further take advantage of the CALIOP resolved profile without having to save the full CALIOP profiles, customized layers defined to integrate with ~~the model~~ (NAAPS) vertical layers were designed specifically for this research and are discussed in Section

15   2.3.2. ~~Here~~, we use CALIOP aerosol products to ~~help~~ verify the NAAPS reanalysis, and CALIOP cloud products to define cloud top heights and screen for thin cirrus.

2.2 Description of model products

The NAAPS reanalysis (Lynch et. al., 2016) is a decade-long (2003-2016) global 1x1 degree and 6-hourly aerosol reanalysis product, which was developed and validated at the Naval Research Laboratory. This reanalysis utilizes a modified version of

20   ~~the~~ NAAPS as its core and assimilates quality-controlled retrievals of AOD from MODIS on Terra and Aqua and the Multi-angle Imaging Spectroradiometer (MISR) on Terra (Zhang et al., 2006; Hyer et al., 2011; Shi et al., 2014). NAAPS characterizes anthropogenic and biogenic fine (including sulfate, and primary and secondary organic aerosols), dust, biomass burning smoke and sea salt aerosols. Smoke from biomass burning is derived from near-real time satellite based thermal anomaly data to construct smoke source functions (Reid et al., 2009), with additional orbital corrections on MODIS based

25   emissions and regional tunings to mitigate missing fire detection resulting from daily variations in orbital coverage and cloud~~s~~ obscuration. Aerosol wet deposition in the tropics is driven by NOAA Climate Prediction Center (CPC) MORPHing (CMORPH) precipitation derived from satellite observations (Joyce et al., 2004) to correct model precipitation biases that ubiquitously exist in numerical models (Xian et al., 2009). The 3-dimensional aerosol fields are resolved vertically into 25 layers between the surface and about ~~70mb~~ following a sigma-pressure coordinate.

30   In addition to NAAPS, the CCARA dataset includes ~~ERA-interim~~ atmospheric reanalysis (or European Reanalysis dataset) (Dee et al., 2011) produced by the European Centre for Medium-Range Weather Forecasts (ECMWF). Meteorological fields such as pressure, temperature, specific and relative humidity, winds, and divergence are included with the CCARA product. Although not used specifically in this paper on ~~simple~~ effective radius sensitivity, the ~~ECMWF~~ reanalysis provides important

Atmospheric
Chemistry
and Physics
Discussions

information on the cloud regional environment. While NAAPS derives its meteorology from NAVGEM, the best and most consistent meteorology in the region is from the ECMWF reanalysis. While this may result in some mismatch between the meteorology and the aerosol components, the key parameters of interest here, including wind shear, water vapor, and temperature profiles, would not substantively impact aerosol-meteorology comparisons and thus the best available data are

5   used.

2.3 Architecture of the collocated MODIS, CALIOP, and NAAPS dataset

The CCARA collocated dataset was processed for the domain of Southeast Asia and the Maritime Continent, specifically $-15°N <$ latitude $< 25°N$ and $90°E <$ longitude $< 140°E$. This dataset spans August 2006 to December 2016, encompassing over ten years of observations and reanalysis. A single collocated footprint was generated at the same size as

10   MODIS native infrared and cloud product spatial resolution (1 km^2) and includes data from MODIS, CALIOP, NAAPS, and ERA-interim reanalysis. First, satellites are collocated, then the gridded model reanalysis is mapped to the collocated satellite dataset. A ten-year dataset was processed starting with data from 2006 through 2016, which includes more than 29 million collocated footprints over SEA. Each footprint contains coincident data from MODIS, CALIOP with the NAAPS and ERA-interim reanalysis. CALIOP, NAAPS, and ERA-interim are vertically resolved and matched to the remote sensing

15   observations as discussed in Section 2.3.1.

2.3.1 Collocation of remote sensing observations and models

The first step to building the collocated dataset is physically collocating the satellite observations, which for this analysis are MODIS and CALIOP whose native resolutions are 1 km^2 and 333 m, respectively. The collocation is run using CALIOP's native Level 1 resolution of 333 m, then down-scaled to match the CALIOP's Level 2 cloud and aerosol products whose resolution is 5 km. The physical collocation methodology assigns a single "master" instrument's observation with

20   subsequent "follower" observations collocated into the master field of view (FOV) (Nagle and Holz, 2009). Typically, the master instrument has the largest surface FOV, which for this dataset is MODIS. The collocation software projects the master FOV (from MODIS) onto the Earth's surface, accounting for the instrument angular FOV and scan angle. Then the software identifies the follower FOVs (from CALIOP) that are coincident with the master observation. Up to four CALIOP

25   333-m FOVs are collocated within a 1-km MODIS footprint as illustrated in Figure 1. Data from each of the CALIOP FOVs are averaged or reported as a fraction (e.g., cloud fraction) and assigned to a single MODIS footprint with the CALIOP data weighted equally. Physically collocating the observations allows for direct intercomparison between the observations including the variability of follower pixels within the MODIS FOV (Nagle and Holz, 2009). We use this variability as a filter to reduce the uncertainty in our analysis as will be discussed in Section 2.4.

30   With the satellites collocated, the NAAPS model fields are added to each MODIS-CALIOP footprint in each file (or *granule)*. Each granule contains approximately 2000 points (the 'along-track' dimension of a MODIS granule). NAAPS and

ERA-interim fields are inserted into existing MODIS-CALIOP FOVs simply by finding and assigning $1° \times 1°$ grid fields to the appropriate MODIS-CALIOP FOV.

2.3.2 Vertical data

Collocating the CCARA ~~data set~~ in the vertical dimension adds significant complexity. CALIOP Level 2 cloud and aerosol
5   layer products provides up to 10 layers defined by the CALIOP feature finding algorithm (Winker et al., 2009). However, the layers' altitudes are dynamic and are not at a high enough vertical resolution to be directly compared to the NAAPS vertical aerosol distributions. In addition to the layer products, the CALIOP Level 2 cloud and aerosol products are also provided as profiles with both the cloud and aerosol extinctions retrieved at 30-m vertical resolution. To facilitate direct comparison between the model fields and the CALIOP cloud and aerosol products, we have defined two sets of customized
10   vertical layers: one that captures the full vertical column at 1-km vertical resolution, and one at slightly higher resolution that captures the planetary boundary layer (PBL).

The first set of layers that captures the full atmospheric column is defined with respect to the mean sea level (MSL). They parse the vertical dimension from 0 – 18 km in 1 km increments (each layer is 1 km in thickness). These are referred to as MSL layers. The second set of layers has a finer vertical resolution and is defined with respect to the surface elevation; these
15   nine layers are referred to as PBL layers. The nine PBL layers, defined with respect to surface elevation, are: 200 – 500 meters, 500 meters – 1 km, 1 – 1.5 km, 1.5 – 2 km, 2 – 2.5 km, 2.5 – 3 km, 3 – 4 km, 4 – 5 km, and 5 – 6 km. The two sets of layers are illustrated in Figure 2. We do not include a 0 – 200 meters layer because the effects of surface reflectance ~~on CALIOP~~ hinder the retrievals (Winker et al., 2009).

For each layer in the MSL and PBL layer sets, NAAPS extinctions and aerosol mass concentrations are interpolated and
20   saved. These are ~~separated by~~ four aerosol species, anthropogenic and biogenic fine mode (or ABF), dust, smoke, and sea salt, and ~~by~~ two aerosol modes, fine or coarse. The CALIOP aerosol and cloud extinction profiles are integrated within each layer providing the layer optical depth. The fractions of cloud or aerosol detected within the layer by CALIOP are also saved. These CALIOP-derived layer products are calculated using the version 3 Level 2 profile products which provide aerosol and cloud extinctions at 30-m resolution. Vertically-resolved ERA-interim meteorology fields (the European
25   Reanalysis Interim data) are also included for the PBL and MSL layers.

2.4 Analytical techniques

This section details the methods of analysis and describes the definition of the First Aerosol Indirect Effect (FAIE) ~~signal~~ using the CCARA dataset. While the dataset has many dimensions of aerosol, cloud and meteorological parameters, for this first introductory paper we are looking at the simple AOD-cloud comparisons, accounting for the deep seated regional biases
30   present in nearly all datasets investigating Southeast Asia (Reid et al., 2013). Future papers will further explore aerosol-cloud indirect effects in SEA.

Input intercomparison: This analysis aims to evaluate the extent to which aerosol particle concentrations and type impact the cloud properties (namely cloud effective radius) of liquid clouds. To this end, we cross-correlated modeled aerosol optical depth anomalies (provided by NAAPS) with cloud r_{eff} (observed by MODIS), using CALIOP to filter for cirrus contamination and provide the cloud top height. As an initial validation of this approach, we first inter-compare the total

5   column AOD between satellite observations and the NAAPS, separating by land and ocean retrievals. AOD innovation is the observed AOD minus the model-derived AOD, or ($AOD_{obs.}-AOD_{NAAPS}$), where the observation can be CALIOP or MODIS. For ocean retrievals, AOD innovations average 0.02 for MODIS-NAAPS and -0.05 for CALIOP-NAAPS. Over land, MODIS-NAAPS innovation has an average of 0.05 compared to 0.07 for CALIOP-NAAPS.

Partitioning the region: Our domain of Southeast Asia is partitioned into oceanic and land sub-regions as we hypothesize

10   different regions of the domain will have varying sensitivities to the FAIE. Ocean retrievals are divided into twenty 10x10-degree grids to analyse the FAIE. To compute thresholds for ocean aerosol anomalies, we use four larger ocean grids to reduce the uncertainty in the anomaly calculation. Land retrievals are divided into six regions which are: 1) Peninsular Southeast Asia (Myanmar, Thailand, Cambodia, Laos, Vietnam); 2) Sumatra and peninsular Malaysia; 3) Borneo, 4) Java, 5) Philippines; and 6) The eastern domain of Sulawesi, Bali, Timor, and New Guinea (hereby East Indonesia). Land aerosol

15   anomaly thresholds are calculated using the same six land regions. Ocean analysis grids and ocean aerosol grids and land regions are shown in Figure 3.

Aerosol anomalies: Like all global aerosol models, it is expected that the NAAPS model has varying regional efficacy. Yet, global models can be expected to simulate large perturbations for large-scale aerosol features (e.g., Sessions et al., 2015) but with poorer fidelity for capturing finer scale local and mesoscale effects. Thus, direct comparisons between the global

20   aerosol model and r_{eff} can lead to regionally varying biases, which in turn can cloud the impact of varying aerosol concentrations on cloud properties. However, perturbations in the large-scale model should reflect regional changes associated with significant biomass burning or anthropogenic pollution events. Thus, cross correlating NAAPS aerosol perturbations to cloud properties can isolate how these large events can influence the cloud environment. Anomalous aerosol amounts were defined by examining the full column fine mode AOD from NAAPS. A scene is determined to be anomalous

25   if the AOD is more or less than an average AOD by one standard deviation. The AOD anomaly thresholds were calculated using the ten-year NAAPS aerosol optical thicknesses that have been mapped to the CCARA product. Distributions of aerosol mass load were divided by species, geographic region, surface type, and season. For each ocean grid and land region, ten-year distributions of aerosol load (integrated aerosol mass concentration) are found separating boreal winter and summer months (i.e. winter is December through May and summer is June through November).

30   *Aerosol thresholds:* Distributions of NAAPS AODs that are collocated into the CCARA dataset are compiled. A mean AOD (μ_{AOD}) and standard deviation of AOD (σ_{AOD}) are calculated and saved for each region and season. We assume distributions of AOD are log-normal, thus μ_{AOD} and σ_{AOD} are the geometric mean and geometric standard deviation of an AOD population. A pixel with NAAPS AOD < (μ_{AOD}/σ_{AOD}) is considered a negative anomalous aerosol event (clean event); AOD > ($\mu_{AOD}*\sigma_{AOD}$) is a positive anomalous aerosol event (polluted event). This threshold definition is such that for each FOV in

the CCARA dataset, there is an assignment of more/less/null aerosol amount for each of the four aerosol species and each of the two aerosol modes. Understandably, different regions experience different clean or polluted seasons due to seasonal and regional patterns biomass burning and land use change (Xian et al., 2013; Reid et al., 2013). Our analysis here uses only the fine mode AOD anomalies.

5   *Filtering*: Distributions of MODIS liquid r_{eff} can be partitioned using a range of criteria such as region and surface type (land or ocean), season, cloud top height, and aerosol anomaly. To identify correlations, bulk "baseline" distributions are calculated that do not filter by any AOD threshold; baseline distributions are meant to serve as a benchmark or control to compare with aerosol anomalous distributions. Cloud top heights are defined using the CALIOP cloud layer product and are divided into three regimes which include layers between 1–3 km (small cumulus), 3–4.5 km (cumulus mediocris), and 4.5–6 km (smaller

10   cumulus congestus), defined above surface elevation. Typically, at 6 km, temperatures are at approximately -5°C, ensuring that clouds are likely not experiencing ice physics. However, clouds at this temperature may be mixed in phase. We use a 6-km height cut-off and liquid-only MODIS retrievals to increase the certainty that we are looking only at liquid water r_{eff} retrievals. CALIOP cloud products are also used to filter FOV with thin ice cirrus contamination above the liquid cloud layer. From these filtered distributions, averages (geometric means) of r_{eff} for baseline, polluted (positive aerosol anomaly),

15   and clean (negative aerosol anomaly) scenarios are calculated. Our goal is to investigate the FAIE by comparing the MODIS r_{eff} for polluted versus clean FOV to the baseline mean r_{eff}. The polluted/clean displacement of r_{eff} from the baseline r_{eff} is called the FAIE signal.

Sampling bias and statistical significance: CALIOP is a nadir-viewing instrument in a polar sun-synchronous orbit. Even with a 10-year record, the sampling statistics when accumulated over small regions for a subset of clouds can be poor. For

20   example, summertime data over the Philippines for land surfaces and clouds existing between 1–3 km yield only 1005 collocated MODIS and CALIOP r_{eff} retrievals. This limited sampling results not just from the nadir viewing geometry, but also the extensive cirrus in the region that attenuate the CALIOP observations and limit the low-level cloud MODIS retrieval yield. After applying an additional filter for investigating the aerosol anomaly, only 40 of those retrievals occur during a positive fine mode aerosol anomaly. For comparison, the 1–3 km summertime clouds in the northernmost and easternmost 1-

25   degree ocean grid have 8603 baseline r_{eff} and 461 retrievals after filtering for positive fine mode aerosol anomaly due to the larger surface area of this region and much higher frequency of low clouds over this ocean grid compared to over the Philippines.

Statistical significance was determined by performing a two-sample t-test on each partitioned distribution of MODIS r_{eff}. The average clean and polluted r_{eff} are compared to the baseline r_{eff}. p-values are calculated and related to means of effective

30   radius. We interpret the p-value to give the certainty that the mean of an anomalous distribution is significantly different from the mean of a baseline distribution. We also specify the type of alternative hypothesis that is tested in the t-test, meaning we can determine to what certainty the mean of an anomalous distribution is more or less than the mean of a baseline distribution. Thus, we can answer specifically whether polluted environments experience smaller cloud droplets than baseline (or "normal") environments. Similarly, we test whether clean environments experience larger mean r_{eff} than

normal environments. We consider any p-value less than 0.01 to signify a significant difference between polluted/clean and baseline distributions.

3 Results

This section focuses on results from the ten-year CCARA dataset over Southeast Asia that includes observations from
5   MODIS and CALIOP as well as NAAPS and ERA-interim reanalysis. Section 3.1 explores the basic properties of the CCARA dataset, including intercomparisons between NAAPS reanalysis aerosol and the CALIOP and MODIS aerosol observations. Then, we ~~compute~~ aerosol anomaly thresholds for each region and ~~season; thresholds are~~ defined using the NAAPS fine mode AOD. We also show the overall mean (or baseline) MODIS effective radius (r_{eff}) for each region and season without considering aerosol anomalies.

10   Section 3.2 investigates the FAIE. To detect ~~the~~ FAIE, we compare populations of baseline r_{eff} to clean and polluted r_{eff}. Statistical significance testing is performed on these populations to determine whether the mean of clean or polluted r_{eff} is greater or less than the mean of the baseline r_{eff} within degree of certainty. To pinpoint when and where the FAIE occurs, populations of r_{eff} are filtered by region (twenty ocean grids and six land regions) and season (winter or summer). Ocean and land regions are shown in Figure 3. To further narrow the occurrence of ~~the~~ FAIE, we filter by other fields in the CCARA
15   dataset such as CALIOP cloud top height.

3.1 Basic data properties

This section details the intercomparison of the NAAPS, MODIS, and CALIOP ~~aerosol optical depths~~ in the ten-year CCARA dataset over Southeast Asia. Here we explore AOD intercomparisons between NAAPS reanalysis and CALIOP and MODIS aerosol observations. We also explore average AOD in each region and season, which we use to define aerosol
20   anomaly thresholds. Lastly, we examine the mean effective radius in each region and season, which we ~~later~~ use in Section 3.2 to explore the FAIE.

3.1.1 Aerosol detection intercomparison: NAAPS versus the observations

An AOD intercomparison between NAAPS and the observing platforms CALIOP and MODIS is presented in Figure 4, showing 2-D histograms of AOD_{MODIS}–AOD_{NAAPS} and AOD_{CALIOP}–AOD_{NAAPS} (aerosol innovations) for the SEA domain
25   with separate distributions for land and ocean retrievals. Recall that the innovation is simply the observed AOD minus the AOD derived from NAAPS reanalysis. Only retrievals where MODIS, CALIOP, and NAAPS all detect non-zero AOD are included. CALIOP was used to filter cirrus contamination and only include cloud-cleared AOD scenes.

Ocean AOD innovations average 0.02 for MODIS–NAAPS and –0.05 for CALIOP–NAAPS. Over ocean, the differences (MODIS–CALIOP) between the observed AOD values average 0.08, much larger than the differences when comparing with
30   <mark>NAAPS ocean AOD</mark>, indicating that the NAAPS bias is small. Over land, MODIS-NAAPS innovation has a mean of 0.05 compared to 0.07 for CALIOP–NAAPS. Land innovations have a wider distribution than ocean innovations for both

Atmospheric
Chemistry
and Physics
Discussions

Open Access

EGU

MODIS–NAAPS and CALIOP–NAAPS. Over land, the MODIS–NAAPS innovations have a variance of 0.04 while the CALIOP–NAAPS innovations have a variance of 0.2. Over ocean, these variances are 0.005 and 0.02 for MODIS–NAAPS and CALIOP–NAAPS, respectively.

The innovations for MODIS–NAAPS are smaller than those for CALIOP-NAAPS; Campbell et al. (2012) states that

5 CALIOP is known to have a low bias. Overall, the AOD biases are small, with NAAPS in generally good agreement with the MODIS and CALIOP observations. NAAPS is understandably in slightly better agreement with MODIS, as the MODIS AOD is assimilated into the NAAPS reanalysis. However, that assimilation occurs less frequently in SEA than in other regions due to persistent cirrus cloud cover. For CALIOP, the retrieval requires assumptions regarding the aerosol lidar ratio which can introduce systematic biases into the AOD retrieval (Campbell et al., 2012).

10 The CCARA dataset provides vertically-distributed NAAPS and CALIOP aerosol extinctions, as discussed in Section 2.3.2. We compare layer extinctions in Figure 5, which present biases and absolute values of aerosol extinction for PBL and MSL layers. For each layer, mean aerosol extinction and mean extinction bias are shown. The bias is the observed layer extinction minus the NAAPS reanalysis layer extinction. Biases separate land and ocean retrievals.

The top panels of Figure 5 show the absolute extinctions (left) and extinction biases (right) for NAAPS and CALIOP MSL

15 layers. Bias is defined as model extinction minus CALIOP observed extinction. Over both ocean and land, NAAPS overestimates CALIOP extinction at higher altitudes, and underestimates CALIOP extinction at lower altitudes. The biases over land are larger than over ocean, consistent with the full-column AOD bias results in Figure 4. The extinction bias switches from positive to negative at 3.5 km over land and 1.5 km over ocean. The bottom panels of Figure 5 show extinctions and extinction biases for the PBL layers, which are a finer vertical resolution near the surface compared to

20 MSL layers. The extinction biases are exaggerated for the finer vertical bins, demonstrating NAAPS's underestimation of CALIOP layer bias over land. The PBL layer closest to the surface reports an extinction bias < -0.07 km^{-1} for land retrievals. In summary, we consider NAAPS aerosol reanalysis in reasonable agreement with MODIS and CALIOP observations. However, NAAPS does demonstrate lower aerosol particle concentrations in the lower free troposphere compared to CALIOP.

25 **3.1.2 Aerosol anomaly threshold definitions**

Aerosol anomalies are defined by calculating the geometric mean (μ_{AOD}) and geometric standard deviation (σ_{AOD}) of NAAPS fine mode aerosol optical thickness for each sub-region and each season (boreal summer, JJASON, and boreal winter, DJFMAM) during all ten years of NAAPS reanalysis collocated into the CCARA data set. The NAAPS fine mode full-column AOD can be thought of as encompassing AOD contributions from both anthropogenic and smoke aerosol

30 species. Because NAAPS AOD are typically log-normally distributed (e.g., Lynch et al., 2016), geometric μ_{AOD} and geometric σ_{AOD} are calculated.

Atmospheric
Chemistry
and Physics
Discussions

We define a positive aerosol anomaly, or polluted event, when the AOD is greater than an upper threshold, ($\mu_{AOD} \times \sigma_{AOD}$). A negative aerosol anomaly, or clean event, is when the AOD is less than a lower threshold, ($\mu_{AOD} \div \sigma_{AOD}$). Winter and summer upper and lower AOD thresholds for each region are shown in Table 1, along with the median AOD values. Recall that to define ocean aerosol anomalies, the region is split into four large grids, which we will distinguish by referring to as

5   southwest, northwest, southeast, and northeast grids. Note the seasonal differences in each region and recall that Indochina experiences a ~~smoky~~ season during winter months while Java, Sumatra, and Borneo experience a ~~smoky~~ season during summer months. These burning seasons are reflected in our AOD thresholds. Summer upper AOD thresholds for Java, Borneo, and Sumatra are much greater than their winter upper thresholds. Over Indochina, the winter upper AOD threshold over double that in the summer.

	Boreal Summer			Boreal Winter		
	$\mu_{AOD}\div\sigma_{AOD}$, median, $\mu_{AOD}\times\sigma_{AOD}$			$\mu_{AOD}\div\sigma_{AOD}$, median, $\mu_{AOD}\times\sigma_{AOD}$		
Land - Indochina	0.06	0.12	0.26	0.10	0.25	0.57
Land - Philippines	0.04	0.08	0.17	0.03	0.07	0.13
Land - E. Indonesia	0.04	0.08	0.15	0.03	0.06	0.11
Land - Java	0.11	0.20	0.32	0.08	0.16	0.28
Land - Borneo	0.06	0.12	0.30	0.05	0.09	0.15
Land - Sumatra	0.06	0.14	0.34	0.07	0.13	0.24
Ocean – south west	0.03	0.07	0.18	0.02	0.04	0.11
Ocean – north west	0.04	0.09	0.20	0.07	0.16	0.33
Ocean – south east	0.03	0.07	0.15	0.02	0.05	0.11
Ocean – north east	0.02	0.05	0.15	0.02	0.06	0.17

10 **Table 1:** Lower fine mode AOD thresholds, median AOD, and upper AOD thresholds, shown for winter and summer for each of the six land regions and four ocean grids. Thresholds were found by computing the geometric mean (μ_{AOD}) and geometric standard deviation (σ_{AOD}). The lower threshold is $\mu_{AOD}\div\sigma_{AOD}$; any AOD below this is considered *clean*. The upper threshold is $\mu_{AOD}\times\sigma_{AOD}$; any AOD above this is *polluted*.

3.1.3 Baseline MODIS effective radius

15 In this section, we show the average (geometric mean or μ_g) MODIS liquid effective radius for each region and season. We also filter effective radius by three cloud height regimes, which are introduced in Section 2.4. These regimes are cloud top heights between 1–3 km, 3–4.5 km, and 4.5–6 km.

An effective radius population with no aerosol anomaly filtering is referred to as a 'baseline' population. Populations of baseline r_{eff} are concatenated for each region and season for the ten-year dataset and the geometric mean of r_{eff} is computed.

20 MODIS liquid r_{eff} retrievals are included only if CALIOP detects no cirrus above the liquid cloud top. Pixels classified as

12

partly cloudy (PCL) by the MODIS cloud mask algorithm (MOD35) are not included to reduce uncertainty in the effective radius results.

Maps of baseline geometric mean r_{eff} are in Figure 6. These maps are shown for each season and cloud height regime. In each map, three black bolded numbers accompany each region. The first signifies the population count and the second

5 preceded by an *s* is the geometric standard deviation of the baseline r_{eff} population. The *s*-number represents the "spread" of the baseline r_{eff} population. The third number is the preceded by an *m* is the median r_{eff}. As expected, average ocean r_{eff} values are larger than land values as oceans regions are typically cleaner environments. ~~Further,~~ r_{eff} is generally larger on the fringes of the domain~~,~~ compared to r_{eff} in the higher populated areas. This is especially true for the ocean grids over the West Pacific, where average r_{eff} commonly exceeds 18 microns, compared to 8–10 microns over densely populated

10 peninsular Southeast Asia and Java. Average r_{eff} values also increase with increasing height, likely resulting from the growth of droplets in deeper clouds. Evidence of major burning seasons in Figure 6 occur over Indochina where the mean r_{eff} for all cloud heights is much smaller during burning active winter compared to summer months. Similar small r_{eff} over Java is seen during summer months. These maps suggest signs of a FAIE. Areas that are known to be polluted/clean experience smaller/larger effective radius retrievals. We now investigate if the mean r_{eff} values are statistically smaller/larger during

15 extreme polluted/clean events in Section 3.2.

3.2 FAIE occurrence

Populations of MODIS liquid r_{eff} are compiled from the CCARA dataset filtering each region and season. We can filter these populations by aerosol thresholds using NAAPS aerosol reanalysis, allowing us to compare clean and polluted r_{eff} populations to baseline r_{eff}, which we consider the 'normal' r_{eff}. The r_{eff} can be filtered by other fields in the CCARA dataset

20 such as CALIOP cloud top height. From the analysis in this section, we establish significant evidence ~~of the~~ FAIE.
Distributions of these populations are shown in Sect. 3.2.1, where clean and polluted r_{eff} are compared to baseline r_{eff}. In Section 3.2.2, we map the mean values of these distributions and investigate whether differences in distributions have statistical significance. Two-sample t-tests are conducted on the data to determine numerically whether means of clean/polluted r_{eff} are significantly larger/smaller than the baseline r_{eff}. Significant FAIE is detected if the two-sample t-test

25 provides a p-value < 0.01.
It is important to distinguish the *direction* of the FAIE. A *polluted FAIE* signifies that r_{eff} is smaller – relative to the region's base line r_{eff} ~~– in cases of excess pollution~~. A *clean FAIE* signal signifies that r_{eff} is larger than the baseline r_{eff} ~~in clean scenes that are lacking aerosol~~.

3.2.1 Populations of r_{eff} for baseline, polluted, and clean cases

30 Distributions of MODIS retrieved r_{eff} were compiled ~~separating~~ each region and season, and cloud height regime. For conciseness, select examples of those distributions are shown in Figure 7. The figure shows normalized distributions of

Atmospheric
Chemistry
and Physics
Discussions

baseline, polluted, and clean r_{eff} of clouds between 1–3 km for six land regions: Indochina and the Philippines in winter and Borneo, Java, East Indonesia, and Sumatra in summer, and as highlighted by the coloured regions in the lower right of Figure 7. Distributions for the West Pacific and Indian Oceans are shown as well. The black lines show the baseline distributions of r_{eff}, i.e. r_{eff} without any aerosol filtering. Note that the baseline distributions vary widely in shape between each region.

5   Panels (a) (Indochina winter) and (e) (Java summer) have baseline r_{eff} with a very small mode and small variance compared to panels (b, c, d, f, h), whose baselines are more widely distributed.

During Boreal winter, drier conditions and enhanced biomass burning are present in the northern half of our study domain. Indochina distributions of r_{eff} are very similar between baseline, polluted, and clean retrievals (a). This suggests that changes in aerosol concentration are not influencing significant change in the effective radius retrievals for the region, even during

10   the burning season. This is unsurprising owing to ~~the regions~~ high levels of biofuel, agricultural waste and industrial emissions (e.g., Reid et al., 2013).   In short, background conditions may already saturate the CCN population. In comparison, the Philippines distributions (b), ~~also in a drier winter period,~~ are different between the baseline, polluted, and clean retrievals during winter months. Polluted Philippines retrievals are smaller than the baseline; clean Philippines retrievals are larger than the baseline. In contrast to Indochina, the Philippines are more sensitive to ~~the~~ FAIE during winter

15   months with the fine mode aerosol concentration impacting the MODIS effective radius retrievals over this region.   Finally, the most dramatic sensitivity ~~is in~~ the West Pacific boreal winter (c), the most remote of the regions examined.

Moving to the boreal summer, the monsoon flips to more wet conditions to the north and ==drier more fire prone conditions== to the south.   In ==Panel D==, Borneo behaves as would be expected owing to its relatively high population, little sensitivity in the baseline and more polluted conditions, but with some residual sensitivity for the "cleanest" of conditions.   Such cleaner

20   conditions do not ~~exit~~ on the highly populated island of Java, with considerably less sensitivity to modeled perturbations in AOD.   Similar findings were found for Sumatra (g).   Some of the largest spreads in r_{eff} for boreal summer were found in the more remote areas, such as Eastern Indonesia over land (f) or the Western Indian ocean – a frequent receptor for pollution from Java (h).

While the examples in Figure 7 hint at signals of clean and polluted FAIE signals, we must consider the statistical

25   significance of these distributions in the comparisons. The next section will systematically explore clean and polluted FAIE signals for each region in SEA and investigate signals of the FAIE where statistical testing has deemed the FAIE significant.

3.2.2 Mapped FAIE for winter and summer

In this section, we compute geometric means of r_{eff} for baseline, polluted, and clean retrievals for each region, season, and cloud height regime. We use a t-test to determine whether the geometric means of those distributions are significantly

30   different from one another to yield a FAIE signal. The significance test is designed such that we can test specifically if the clean r_{eff} is *larger* than the baseline r_{eff} (a clean FAIE) and if the polluted r_{eff} is *smaller* than the baseline r_{eff} (polluted FAIE). The magnitude of the FAIE is the displacement of the anomalous (clean or polluted) r_{eff} from the baseline r_{eff}:

$$\text{clean FAIE} = \text{clean } r_{eff} - \text{baseline } r_{eff} \geq 0$$

$$\text{polluted FAIE} = \text{polluted } r_{eff} - \text{baseline } r_{eff} \leq 0$$

This definition is defined so the clean FAIE is positive in sign and the polluted FAIE is negative. Figure 8 shows maps of average r_{eff} values for baseline populations, as well as maps of polluted and clean FAIE signals during summer months.

5   Winter months are shown in Figure 9. The rows in this figure signify different cloud top height regimes; the columns show the baseline r_{eff}, polluted FAIE signal, and clean FAIE signal. The cloud height regimes signified by the rows in Figures 8 and 9 correlate from bottom to top: 1–3 km, 3–4.5 km, and 4.5–6 km. The FAIE signal maps are only shaded if the FAIE is deemed statistically significant (p < 0.01). Note that the same region may yield a significant clean FAIE but not a significant polluted FAIE, or vice versa.

10   During winter months shown in Figure 9, for clouds nearest to the surface (between 1–3 km) there is a significant clean and polluted FAIE (up to 6 microns in magnitude) for the West Pacific Ocean retrievals, just east of the Philippines. This suggests that under heavily polluted environments, the average effective radius is up to 6 microns smaller relative to the effective radius under every-day scenes. Under extremely clean scenes, the average effective radius can be over 5 microns larger than the bulk average. Even for high clouds at 4.5–6 km, a polluted and clean FAIE signal is found for some of the

15   West Pacific grids. A polluted and clean FAIE is also present for the Eastern Indian Ocean. A very weak (< 1 micron in magnitude) clean and polluted FAIE signal exists for low clouds over Indochina. These FAIE signals are weak as the environment is likely almost always saturated with fine mode aerosol, resulting in additional sources having limited impact on the water cloud droplet size. Comparing Indochina in Figure 8 to Panel (a) in Figure 7, note that while the normalized histograms of clean and polluted r_{eff} are almost identical, the slight difference in the right-side tails of this distribution, in

20   addition to the high number of counts, yields a p-value small enough to consider this difference significant. The example of wintertime Indochina is consistent with the notion that there is a physical upper limit to cloud-aerosol interactions (Painemal and Zuidema, 2013). A slightly stronger FAIE over Indochina does appear for higher altitude clouds, though the average r_{eff} for all (baseline) clouds over Indochina stays quite small and does not exceed 12 microns even for the tallest clouds. The black bolded numbers in Figures 8 and 9 signify the count of the cloud populations for each region in each panel. The

25   purpose of showing these counts is to indicate whether the lack of a FAIE signal is due to low cloud counts or an insignificant change in the average anomalous r_{eff}.

Over some West Pacific peripheral ocean regions in Figure 9, there is a lack of polluted liquid r_{eff} retrievals for higher clouds (3–6 km). One reason for this is that the region is regularly covered in cirrus, reducing the likelihood of a liquid retrieval from MODIS. Additionally, while significant smoke and pollution can reach this region, it is somewhat rare and

30   compounded by how we defined aerosol anomaly. Our aerosol thresholds were defined by determining whether a certain AOD amount was anomalous relative to all clouds in that region during that season, *not* answering whether the AOD was anomalous to specific cloud top heights in that region during that season. Further, recall that ocean aerosol anomalies are determined for larger ocean grids, not the small 10x10-deg grids in Figures 8 and 9. For these reasons, it follows that some

easternmost West Pacific polluted FAIE grids in Figure 9 indicate a "0" count for taller cloud height regimes because any anomalously polluted clouds in that region are mostly likely to exist in the lowest regime closest to the surface.

During summer months shown in Figure 8, a strong polluted FAIE appears across the SEA domain. Significant clean FAIE signals are present as well. Peripheral ocean regions in the West Pacific (upper right in maps) and Indian Ocean (lower left in
5   maps) experience a strong polluted FAIE, with clouds decreasing in average r_{eff} up to 6 microns for all cloud height regimes. It is clear that the burning season of Sumatra, Java, and Borneo has a great effect on cloud droplet size over ocean regions, with far-reaching effects into the West Pacific. It is likely that the nearly constant presence of anthropogenic aerosols from Indochina have an effect on West Pacific effective radius retrievals as well.

There is a complete absence of polluted FAIE signals over Java, Sumatra, and Borneo for 1–3 km clouds. These land regions
10   have large populations, significant biofuel usage, and undergo burning seasons during these months. Java yields no polluted FAIE signal for *any* cloud heights. The mean r_{eff} values in baseline and clean cases over Java are relatively low at 13 microns, implying that these regions are saturated with aerosol particles; relative changes in the aerosol loading having minimal effect on cloud droplet sizes.

4 Discussion and conclusions

15   Southeast Asia and the Maritime Continent have long been thought of as particularly vulnerable to climate change. High population density and proximity to remote ocean regions highlights the complexity of observing aerosol indirect effects in this region. In this analysis, we have shown that the effects of anthropogenic and smoke aerosols on cloud properties are detectable using the ten-year collocated Curtain Cloud-Aerosol Regional A-Train (CCARA) dataset, which includes data from MODIS and CALIOP and model reanalysis from the NAAPS. The dataset uses aerosol reanalysis from NAAPS paired
20   with concurrent satellite cloud observations to show significant signs of a first aerosol indirect effect or FAIE. This effect occurs when the mean effective radius is larger in anomalously clean cases and smaller in anomalously polluted cases when comparing to the overall (baseline) average r_{eff}. We call these effects the clean FAIE and polluted FAIE signals, respectively. FAIE signals are significant only if the r_{eff} populations of anomalous and clean scenes pass a significance t-test and yield p-values < 0.01.

25   Section 3.2.2 shows that clean and polluted FAIE signals are quite common throughout the SEA domain during both winter and summer. Disregarding r_{eff} in scenes of aerosol anomaly, baseline average r_{eff} can vary greatly between regions. Biomass burning seasons are reflected in the baseline r_{eff}, as distributions of r_{eff} are often condensed to very small values over land, as shown in examples in Figure 6. Furthermore, burning seasons cause saturation in CCN for low clouds (1–3 km) over land. In these regions, changes in pollution have a limited impact on observed effective radius.

30   Smoke burning and anthropogenic aerosols have long-reaching effects on cloud properties in SEA. Figures 8 and 9 show that peripheral ocean regions are often times the most affected by influxes of anthropogenic aerosol; this is seen in winter and summer months. The region is clearly sensitive to the FAIE even in areas that are thought of as remote or pristine. There is

Atmospheric
Chemistry
and Physics
Discussions

often a weak or nonexistent FAIE over regions that are saturated with aerosol, i.e. low clouds (cloud top height 1–3 km) over burning polluted land areas. This is seen for Sumatra, Java, and Borneo during summer months and for Indochina during winter months. This result signifies that under high pollution events in already polluted regions, changes in aerosol amount have little to no effect on cloud microphysics. These same regions do sometimes yield a polluted FAIE for high liquid water

5 clouds (cloud top height 4.5–6 km), signifying that the FAIE has some sensitivity to cloud height.

Our results show significant and consistent signs of correlation between observed liquid water droplet size (from MODIS r_{eff}) and aerosol amount (from NAAPS aerosol reanalysis). Smaller effective radius retrievals are associated with a surplus of aerosol (polluted events) while larger effective radius retrievals are associated with a lack of aerosol (clean scenarios). These correlations depend on location and surface type, time of year, and cloud top altitude. An important finding from this

10 analysis is that anthropogenic aerosol emissions in SEA have far-reaching impacts on cloud properties, affecting even high clouds in remote ocean regions that are often thought of as pristine. A clean and polluted FAIE is common throughout the domain. The FAIE appears strongest in peripheral ocean regions such as the south Indian Ocean and western Pacific Ocean, east of the Philippines. We have concluded that the utilization of a ten-year collocated dataset that combines satellite cloud observations with modeling fields is a unique method to obtain statistically significant evidence of the FAIE. We hope this

15 study will serve as a precursor to investigating the indirect effects of aerosol on precipitation, or the second aerosol indirect effect (SAIE). We draw the connection between the FAIE and SAIE under the premise that in order for aerosol to affect precipitation processes in cumulus clouds, they first have to affect cloud droplet size.

References

Ackerman, S. A., Strabala, K. I., Menzel, W. P., Frey, R. A., Moeller, C. C., and Gumley, L. E.: Discriminating clear sky from clouds with MODIS, J. Geophys. Res., 103(D24), 32141–32157, doi:10.1029/1998JD200032, 1998.

Campbell, J. R., Reid, J. S., Westphal, D. L., Zhang, J., Tackett, J. L., Chew, B. N., Welton, E.J., Shimizu, A., Sugimoto, N.,
30 Aoki, K., Winker, D. M.: Characterizing the vertical profile of aerosol particle extinction and linear depolarization over Southeast Asia and the Maritime Continent: The 2007–2009 view from CALIOP, Atmo. Res., 122, 520-543, doi:10.1016/j.atmosenv.2011.08.017, 2013.

Atmospheric
Chemistry
and Physics
Discussions

Chew, B. N., Campbell, J. R., Reid, J. S., Giles, D. M., Welton, E. J., Salinas S. V., and Liew S. C.: Tropical cirrus cloud contamination in sun photometer data, Atmos. Environ., 45, 6724-6731, doi:10.1016/j.atmosenv.2011.08.017, 2011.

Cruz, R.V., Harasawa, H., Lal, M., Wu, S., Anokhin, Y., Punsalmaa, B., Honda, Y., Jafari, M., Li, C. and Huu Ninh, N.: Chapter 10: Asia, in: IPCC Fourth Assessment Report, edited by Parry, M.L., Canziani, O.F., Palutikof, J.P., van der Linden, 5 P.J.and Hanson, C.E., Cambridge University Press, Cambridge, 469-506, 2007.

Cruz, F. T., Narisma, G. T., Villafuerte II. M., Olaguera L. M. P., A climatological analysis of the southwest monsoon rainfall in the Philippines, Atmo. Res., 122, 609-616, doi:10.1016/j.atmosres.2012.06.010, 2013.

Dee, D. P., Uppala, S. M., Simmons, A. J., Berrisford, P., Poli, P., Kobayashi, S., Andrae, U., Balmaseda, M. A., Balsamo, G., Bauer, P., Bechtold, P., Beljaars, A. C. M., van de Berg, L., Bidlot, J., Bormann, N., Delsol, C., Dragani, R., Fuentes, M., 10 Geer, A. J., Haimberger, L., Healy, S. B., Hersbach, H., Hólm, E. V., Isaksen, L., Kållberg, P., Köhler, M., Matricardi, M., McNally, A. P., Monge-Sanz, B. M., Morcrette, J.-J., Park, B.-K., Peubey, C., de Rosnay, P., Tavolato, C., Thépaut, J.-N. and Vitart, F.: The ERA-Interim reanalysis: configuration and performance of the data assimilation system, Q.J.R. Meteorol. Soc., 137, 553–597, doi:10.1002/qj.828, 2011.

Graf, H.-F., Yang, J., and Wagner, T. M.: Aerosol effects on clouds and precipitation during the 1997 smoke episode in 15 Indonesia, Atmos. Chem. Phys., 9(2), 743-756, doi:10.5194/acp-9-743-2009, 2009.

Hijioka, Y., Lin, E., Pereira, J.J., Corlett, R.T., Cui, X., Insarov, G.E., Lasco, R.D., Lindgren, E., Surjan, and A.: Chapter 24: Asia, in: IPCC Fifth Assessment Report, edited by Barros, V.R., Field, C.B., Dokken, D.J., Mastrandrea, M.D., Mach, K.J., Bilir, T.E., Chatterjee, M., Ebi, K.L., Estrada, Y.O., Genova, R.C., Girma, B., Kissel, E.S., Levy, A.N., MacCracken, S., Mastrandrea, P.R., and White, L.L., Cambridge University Press, Cambridge, 1327-1370, 2013.

20 Hyer, E. J., Reid, J. S., and Zhang, J.: An over-land aerosol optical depth data set for data assimilation by filtering, correction, and aggregation of MODIS Collection 5 optical depth retrievals, Atmos. Meas. Tech., 4(3), 379-408, doi:10.5194/amt-4-379-2011, 2011.

Joyce, R. J., Janowiak, J. E., Arkin, P. A., & Xie, P.: CMORPH: A method that produces global precipitation estimates from passive microwave and infrared data at high spatial and temporal resolution, J. Hydrometeorol., 5(3), 487-503, 25 doi:10.1175/1525-7541(2004)005<0487:CAMTPG>2.0.CO;2, 2004.

Langmann, B.: A model study of smoke-haze influence on clouds and warm precipitation formation in Indonesia 1997/1998, Atmos. Environ., 41(32), 6838-6852, doi:10.1016/j.atmosenv.2007.04.050, 2007.

Lynch, P., Reid, J.S., Westphal, D.L., Zhang, J., Hogan, T.F., Hyer, E.J., Curtis, C.A., Hegg, D.A., Shi, Y., Campbell, J.R. and Rubin, J.I.: Development studies towards an 11-year global gridded aerosol optical thickness reanalysis for climate and 30 applied applications, *Geosci. Model Dev. Discuss.,* 8(12), doi:10.5194/gmdd-8-10455-2015, 2015.

Lynch, P., Reid, J.S., Westphal, D.L., Zhang, J., Hogan, T.F., Hyer, E.J., Curtis, C.A., Hegg, D.A., Shi, Y., Campbell, J.R., Rubin, J.I., Sessions, W.R., Turk, F.J., and Walker, A.L.: An 11-year global gridded aerosol optical thickness reanalysis (v1. 0) for atmospheric and climate scietnces, Geosci. Model Dev., 9, 1489–1522, doi:10.5194/gmd-9-1489-2016, 2016.

Nagle, F. W. and Holz, R. E.: Computationally efficient methods of collocating satellite, aircraft, and ground observations, J.
5   Atmos. Oceanic Tech., 26(8), 1585-1595, doi:10.1175/2008JTECHA1189.1, 2009.

Painemal, D. and Zuidema, P.: The first aerosol indirect effect quantified through airborne remote sensing during VOCALS-REx, Atmos. Chem. Phys., 13(2), 917-931, doi:10.5194/acp-13-917-2013, 2013.

Platnick, S., Meyer, K.G., King, M.D., Wind, G., Amarasinghe, N., Marchant, B., Arnold, G.T., Zhang, Z., Hubanks, P.A., Holz, R.E., Yang, P., Ridgway, W.L., and Reidi, J.: The MODIS cloud optical and microphysical products: Collection 6
10 updates and examples from Terra and Aqua, IEEE Trans. Geosci. Remote Sens., 55(1), 502-525, doi:10.1109/TGRS.2016.2610522, 2017.

Reid, J.S., Hyer, E.J., Prins, E.M., Westphal, D.L., Zhang, J., Wang, J., Christopher, S.A., Curtis, C.A., Schmidt, C.C., Eleuterio, D.P., Richardson, K.A., and Hoffman, J.P.: Global monitoring and forecasting of biomass-burning smoke: Description of and lessons from the Fire Locating and Modeling of Burning Emissions (FLAMBE) program, IEEE J. Sel.
15 Top. Appl. Earth. Obs. Remote Sens., 2(3), 144-162, doi:10.1109/JSTARS.2009.2027443, 2009.

Reid, J.S., Xian, P., Hyer, E.J., Flatau, M.K., Ramirez, E.M., Turk, F.J., Sampson, C.R., Zhang, C., Fukada, E.M. and Maloney, E.D.: Multi-scale meteorological conceptual analysis of observed active fire hotspot activity and smoke optical depth in the Maritime Continent, Atmos. Chem. Phys., 12(4), 2117-2147, doi:10.5194/acp-12-2117-2012, 2012.

Reid, J.S., Hyer, E.J., Johnson, R.S., Holben, B.N., Yokelson, R.J., Zhang, J., Campbell, J.R., Christopher, S.A., Di
20 Girolamo, L., Giglio, L., Holz, R.E., Kearney, C., Miettinen, J., Reid, E.A., Turk, F.J., Wang, J., Xian, P., Zhao, G., Balasubramaniann, R., Boon, N.C., Janjai, S., Lagrosas, N., Lestari, P., Lin, N., Mahmud, M., Nguyen, A.X., Norris, B., Oanh, N.T.K., Oo, M., Salinas, S.V., Welton, E.J., and Liew, S.C.: Observing and understanding the Southeast Asian aerosol system by remote sensing: An initial review and analysis for the Seven Southeast Asian Studies (7SEAS) program, Atmos. Res., 122, 403-468, doi:10.1016/j.atmosres.2012.06.005, 2013.

25 Reid, J. S., Lagrosas, N. D., Jonsson, H. H., Reid, E. A., Sessions, W. R., Simpas, J. B., Uy, S. N., Boyd, T. J., Atwood, S. A., Blake, D. R., Campbell, J. R., Cliff, S. S., Holben, B. N., Holz, R. E., Hyer, E. J., Lynch, P., Meinardi, S., Posselt, D. J., Richardson, K. A., Salinas, S. V., Smirnov, A., Wang, Q., Yu, L., and Zhang, J.: Observations of the temporal variability in aerosol properties and their relationships to meteorology in the summer monsoonal South China Sea/East Sea: the scale-dependent role of monsoonal flows, the Madden–Julian Oscillation, tropical cyclones, squall lines and cold pools, Atmos.
30 Chem. Phys., 15, 1745-1768, doi:10.5194/acp-15-1745-2015, 2015.

Atmospheric
Chemistry
and Physics
Discussions

Open Access

Reid, J. S., Lagrosas, N. D., Jonsson, H. H., Reid, E. A., Atwood, S. A., Boyd, T. J., Ghate, V. P., Xian, P., Posselt, D. J., Simpas, J. B., Uy, S. N., Zaiger, K., Blake, D. R., Bucholtz, A., Campbell, J. R., Chew, B. N., Cliff, S. S., Holben, B. N., Holz, R. E., Hyer, E. J., Kreidenweis, S. M., Kuciauskas, A. P., Lolli, S., Oo, M., Perry, K. D., Salinas, S. V., Sessions, W. R., Smirnov, A., Walker, A. L., Wang, Q., Yu, L., Zhang, J., and Zhao, Y.: Aerosol meteorology of Maritime Continent for

5   the 2012 7SEAS southwest monsoon intensive study – Part 2: Philippine receptor observations of fine-scale aerosol behavior, Atmos. Chem. Phys., 16, 14057-14078, doi:10.5194/acp-16-14057-2016, 2016.

Rosenfeld, D., Andreae, M.O., Asmi, A., Chin, M., Leeuw, G., Donovan, D.P., Kahn, R., Kinne, S., Kivekäs, N., Kulmala, M. and Lau, W.: Global observations of aerosol-cloud-precipitation-climate interactions, Rev. Geophys., 52, 750–808, doi:10.1002/2013RG000441, 2014.

10   Salomonson, V.V., Barnes, W., Xiong, J., Kempler, S. and Masuoka, E.: An overview of the Earth Observing System MODIS instrument and associated data systems performance, In Geoscience and Remote Sensing Symposium, 2002. IGARSS'02. 2002 IEEE International, 2, 1174-1176), doi:10.1109/IGARSS.2002.1025812, 2002.

Sessions, W.R., Reid, J.S., Benedetti, A., Colarco, P.R., da Silva, A., Lu, S., Sekiyama, T., Tanaka, T.Y., Baldasano, J.M., Basart, S. and Brooks, M.E.: Development towards a global operational aerosol consensus: basic climatological

15   characteristics of the International Cooperative for Aerosol Prediction Multi-Model Ensemble (ICAP-MME), Atmos. Chem. Phys., 15, 335-362, doi:10.5194/acp-15-335-2015, 2015.

Sharma, D. and Babel, M. S.: Trends in extreme rainfall and temperature indices in the western Thailand, Int. J. Climatol., 34: 2393–2407. 2014 doi: 10.1002/joc.3846, 2014.

Shi, Y., Zhang, J., Reid, J.S., Liu, B. and Hyer, E.J.: Critical evaluation of cloud contamination in the MISR aerosol products

20   using MODIS cloud mask products, Atmos. Meas. Tech., 7(6), 1791-1801, 2014.

Sorooshian, A., Feingold, G., Lebsock, M. D., Jiang, H., and Stephens, G. L.: Deconstructing the precipitation susceptibility construct: Improving methodology for aerosol- cloud precipitation studies, J. Geophys. Res., 11(5), D17201, doi:10.1029/2009JD013426, 2010.

Twomey, S.: The influence of pollution on the shortwave albedo of clouds, J. Atmos. Sci., 34(7), 1149-1152, doi:

25   10.1175/1520-0469(1977)034<1149:TIOPOT>2.0.CO;2, 1977.

Twomey, S.: Pollution and the planetary albedo. Atmos. Environ. (1967), 8(12), 1251-1256, doi:10.1016/0004-6981(74)90004-3, 1974.

Winker, D.M., Vaughan, M.A., Omar, A., Hu, Y., Powell, K.A., Liu, Z., Hunt, W.H. and Young, S.A.: Overview of the CALIPSO mission and CALIOP data processing algorithms. Journal of Atmospheric and Oceanic Technology, 26(11),

30   doi:10.1175/2009JTECHA1281.1, 2310-2323, 2009.

Xian, P., Reid, J.S., Turk, J.F., Hyer, E.J. and Westphal, D.L.: Impact of modeled versus satellite measured tropical precipitation on regional smoke optical thickness in an aerosol transport model, Geophys. Res. Lett., 36(16), doi:10.1029/2009GL038823, 2009.

Xian, P., Reid, J. S., Atwood, S. A., Johnson, R. S., Hyer, E. J., Westphal, D. L., and Sessions, W.: Smoke aerosol transport
5   patterns over the Maritime Continent, Atmos. Res., 122, 469-485, doi:10.1016/j.atmosres.2012.05.006, 2013.

Yuan, T., Remer, L. A., Pickering, K. E., and Yu, H.: Observational evidence of aerosol enhancement of lightning activity and convective invigoration, Geophys. Res. Lett., 38, L04701, doi:10.1029/2010GL046052, 2011.

Zhang, J. and Reid, J.S.: MODIS aerosol product analysis for data assimilation: Assessment of over-ocean level 2 aerosol optical thickness retrievals. J. Geophys. Res.: Atmos., 111(D22), doi:10.1029/2005JD006898, 2006.

10
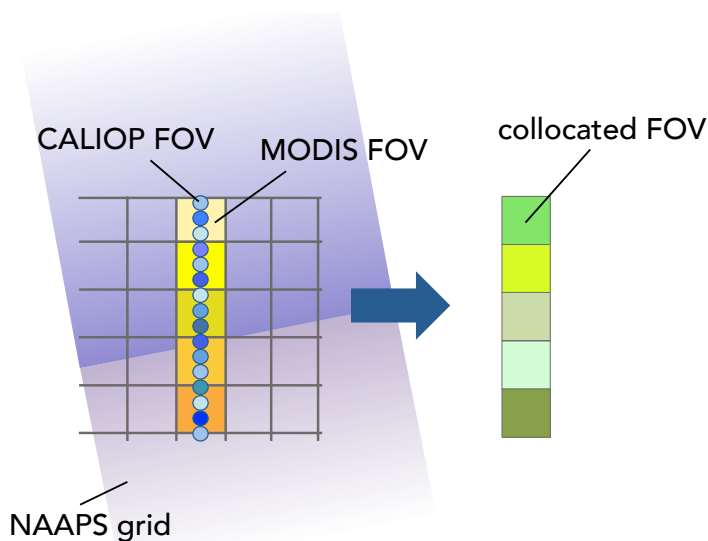
Figure 1: Schematic showing the collocation process matching MODIS, CALIOP, and NAAPS. Multiple CALIOP fields of view
15   **(FOV) are mapped to a single MODIS FOV and averaged. Each satellite FOV is then assigned a NAAPS grid that is closest in space and time. This process is repeated for ten years of A-Train orbit to compose the CCARA dataset.**
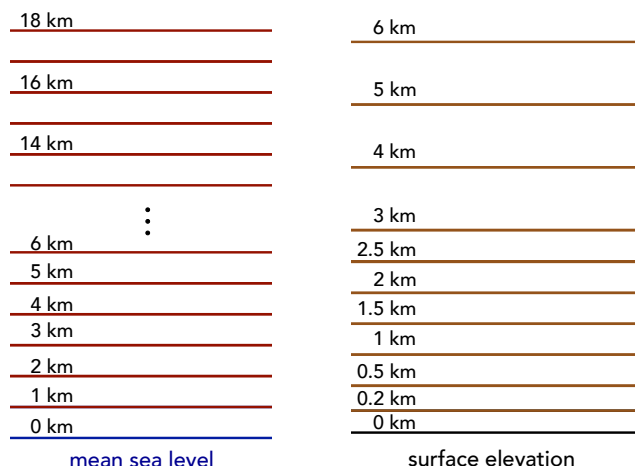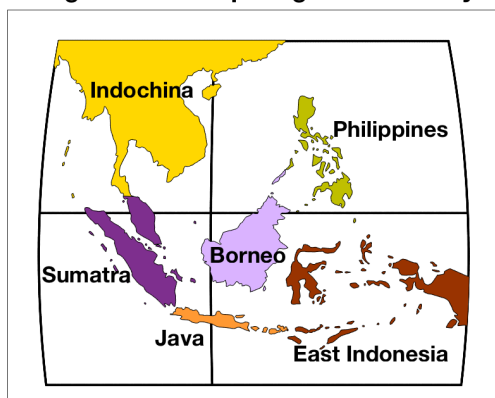
Figure 2: The vertical layers saved in the CCARA dataset. Left – mean sea level layers (MSL layers) are defined with respect to sea level and capture the full atmospheric column. Right – planetary boundary layer layers (PBL layers) are defined with respect to surface elevation and capture the boundary layer.
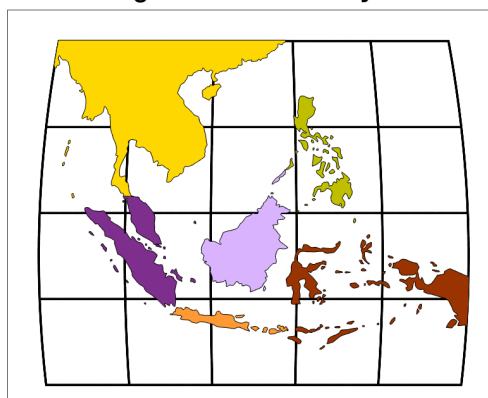

5

Figure 3: Regions for computing AOD anomaly thresholds (left) and regions for investigating the FAIE (right). For land, the same regions are used for both AOD anomaly calculations and for the FAIE analysis. For ocean, we perform the FAIE analysis on twenty 10x10-degree grids, but aerosol anomaly thresholds for ocean regions are found using four larger grids, shown in the left plot. Land regions are distinguished with unique colors: Indochina in yellow, the Philippines in green, East Indonesia in dark red,
10 **Java in orange, Borneo in lavender, and Sumatra in purple.**

Atmospheric
Chemistry
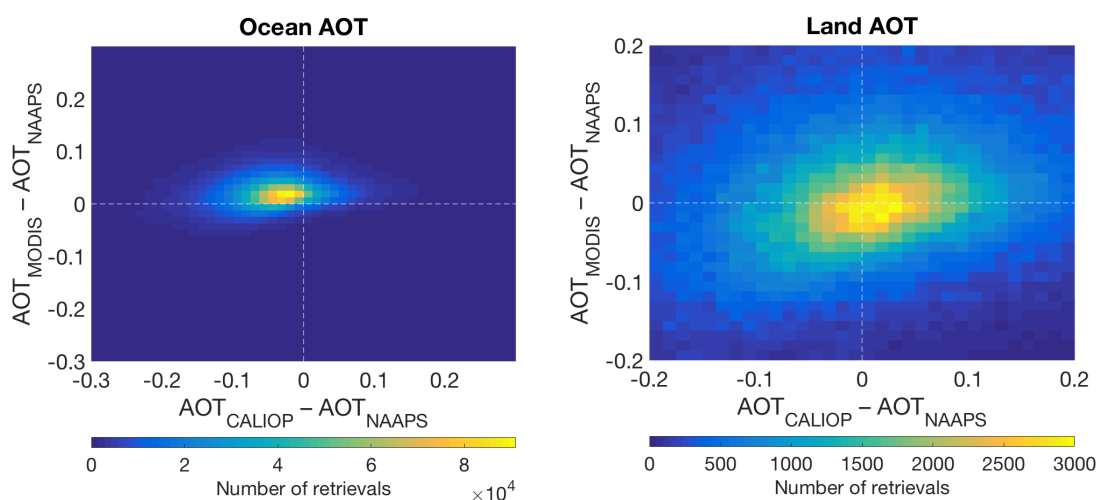and Physics
Discussions

Figure 4: 2D histogram of AOD innovations for ocean retrievals (left) and land retrievals (right) over Southeast Asia during 2006-2016. AOD_{CALIOP} minus AOD_{NAAPS} is shown on the x-axis and AOD_{MODIS} minus AOD_{NAAPS} is shown on the y-axis. The color scale represents the count of retrievals in each bias bin. Only cloud-cleared pixels classified by both MODIS and CALIOP are included. Only pixels where NAAPS, MODIS, and CALIOP all detect non-zero AOD are included.
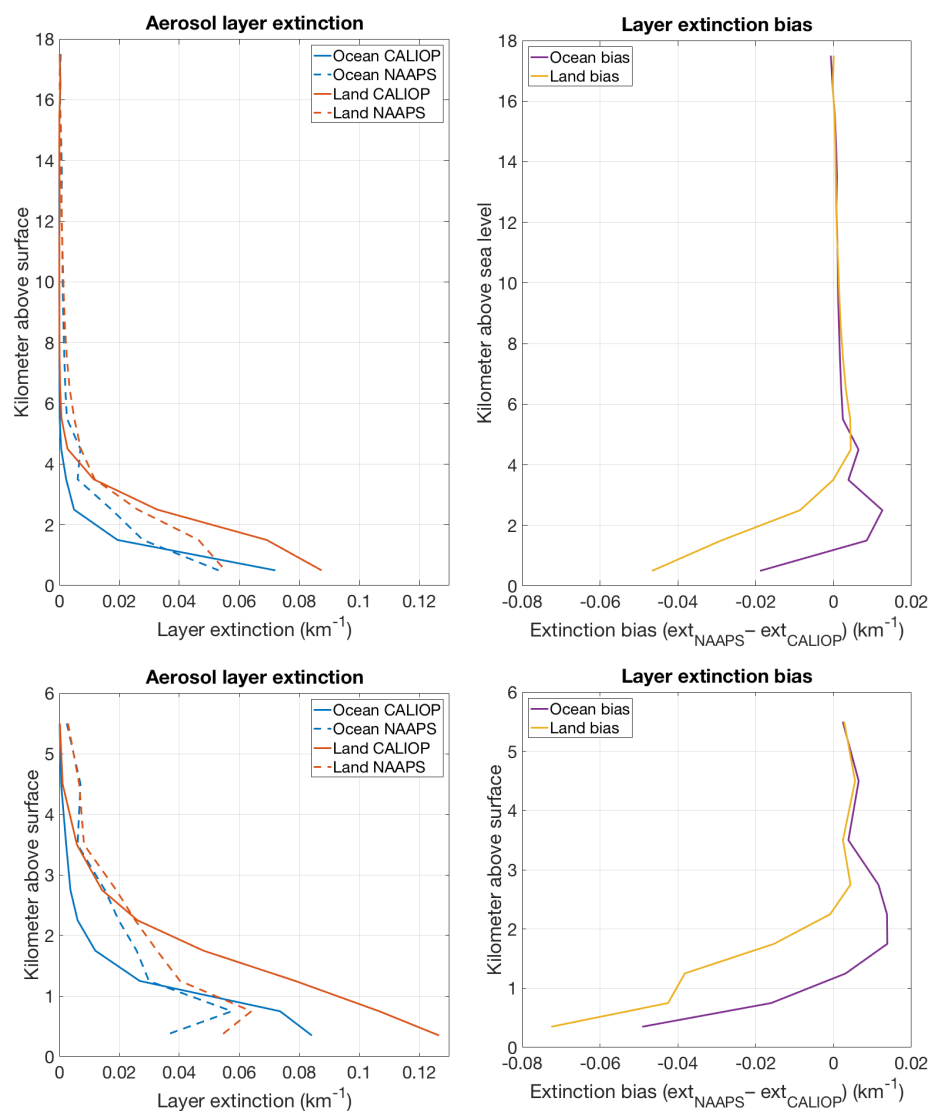
Figure 5: Vertical layer distributions of average CALIOP and NAAPS aerosol extinctions (left panels) and vertical distributions of CALIOP − NAAPS extinction bias (right panels). Extinctions and extinction biases are shown for PBL layers (bottom panels) and MSL layers (top panels). Layer extinction averages are for all SEA retrievals during 2006-2016. Only CALIOP cloud-cleared pixels and pixels where NAAPS and CALIOP detect positive total AOD are included.
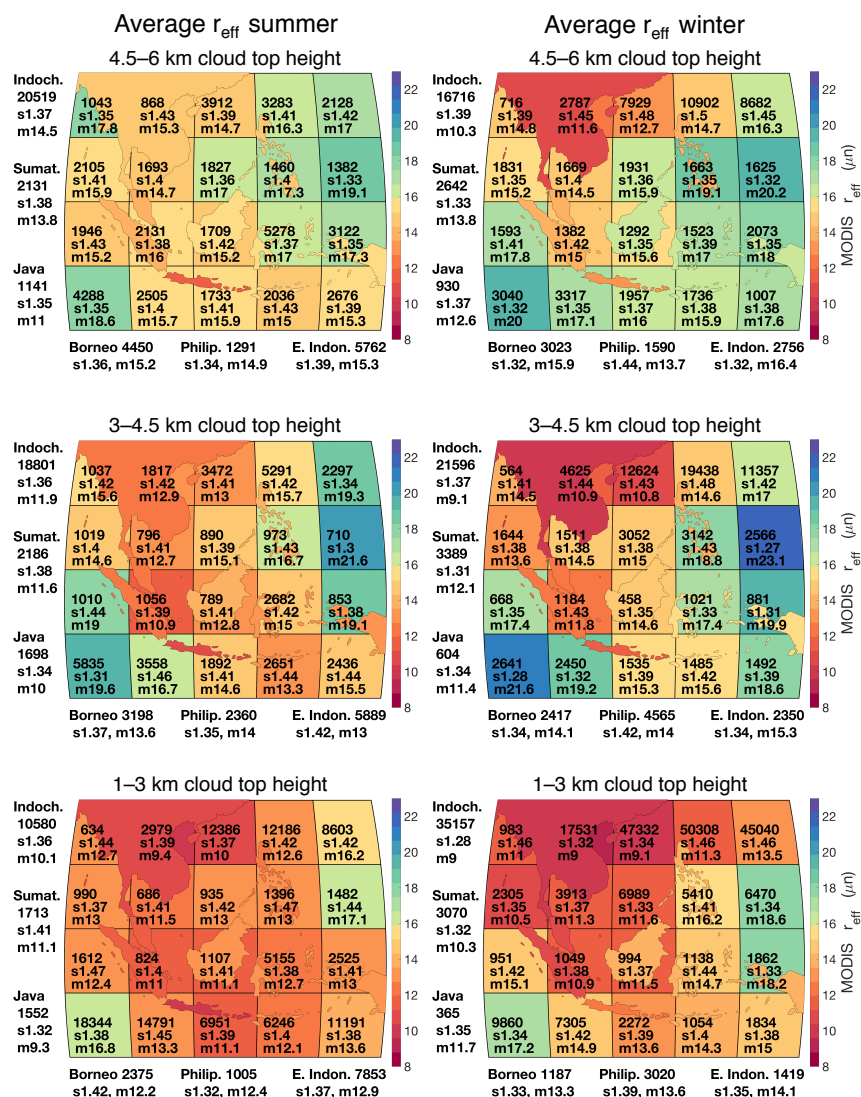
Atmospheric
Chemistry
and Physics
Discussions

Figure 6: Geometric means and standard deviations of baseline r_{eff} for each ocean grid and land region for summer (left column) and winter (right column) spanning 2006 to 2016 for three cloud height regimes. The rows show the three cloud height regimes that are classified using CALIOP. Bottom panels show clouds with tops at 1-3 km in height, middle panels show clouds at 3-4.5 km, and top panels show clouds at 4.5-6 km. The color scale is the geometric mean of the effective radius (in microns); the color scale range is the same for each panel. Each region is accompanied by three black bolded numbers, the first shows the number of counts in each r_{eff} population, the second is the geometric standard deviation of each population (preceded by an 's'), the third value is the median of the r_{eff} population (preceded by an 'm').
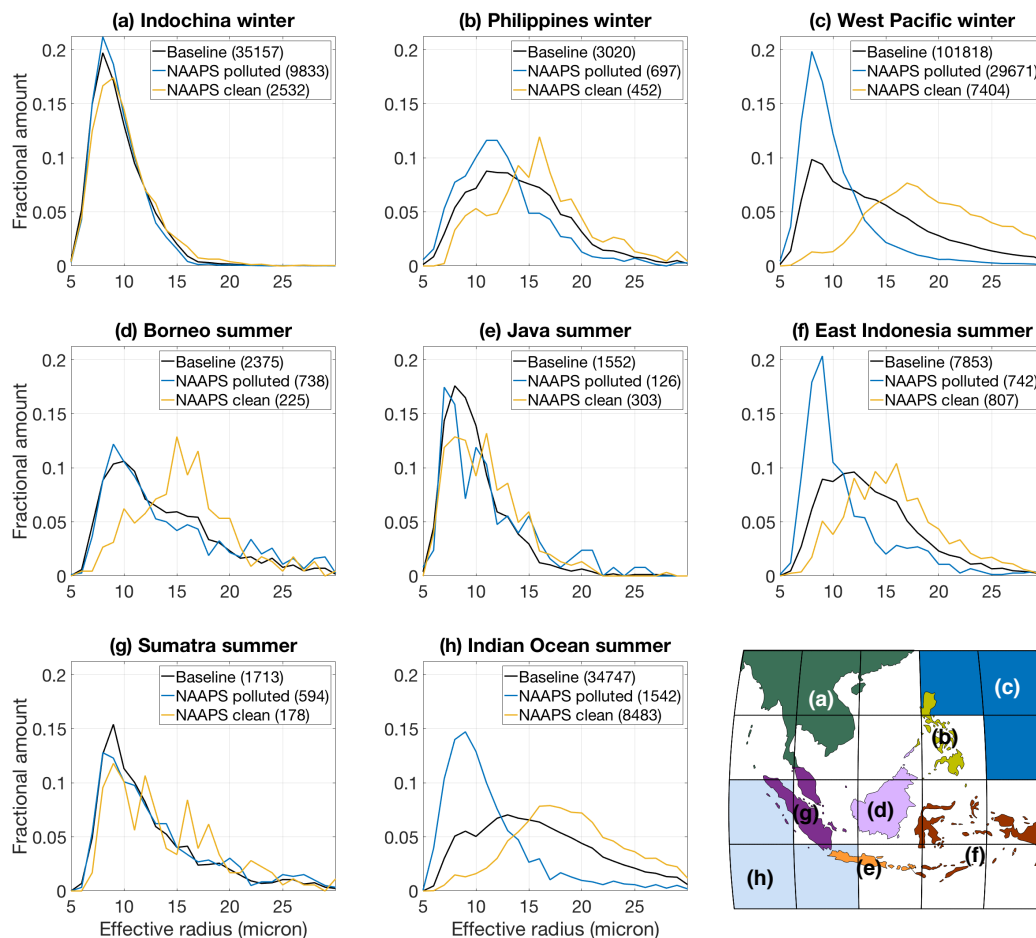
Figure 7: Normalized distributions of MODIS effective radius for baseline, polluted, and clean retrievals showing six regions in panels (a) through (h): Indochina, the Philippines, and the West Pacific Ocean during winter and Borneo, Java, East Indonesia, Sumatra, and the Indian Ocean during summer. Each panel has the same x- and y-axis scale, where the y-axis shows the fractional amount of clouds. Counts of each population are shown in parentheses in the legends. A map in the lower left is provided as a reference to show each region.
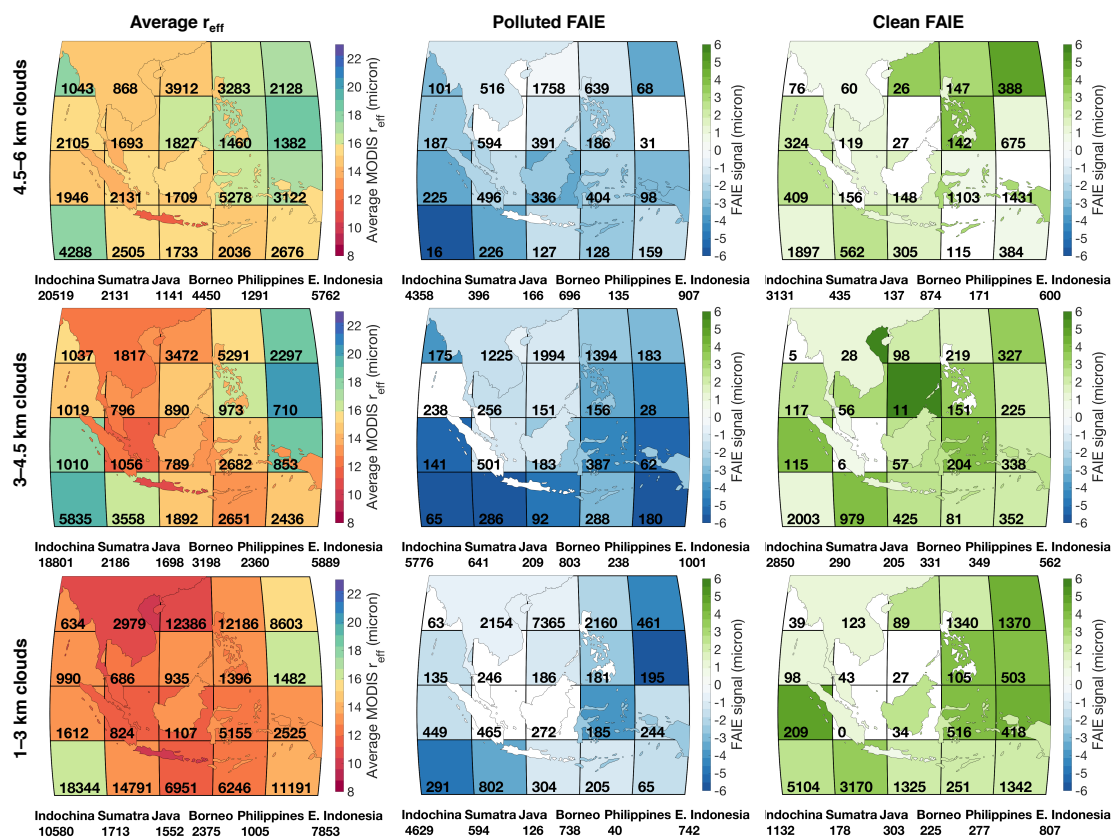
Atmospheric
Chemistry
and Physics
Discussions
Open Access
EGU

Figure 8: Maps illustrating average baseline r_{eff} and significant polluted and clean FAIE signals. Summer months June through November are shown here. The columns from left to right show the average bulk (or baseline) r_{eff}, significant polluted FAIE, and significant clean FAIE. The rows from bottom to top show cloud top height regimes: clouds between $1 - 3$ km, $3 - 4.5$ km, and $4.5 - 6$ km. Polluted and clean FAIE signals are shaded only if the significance t-test between baseline and anomalous r_{eff} populations yields a p-value < 0.01.
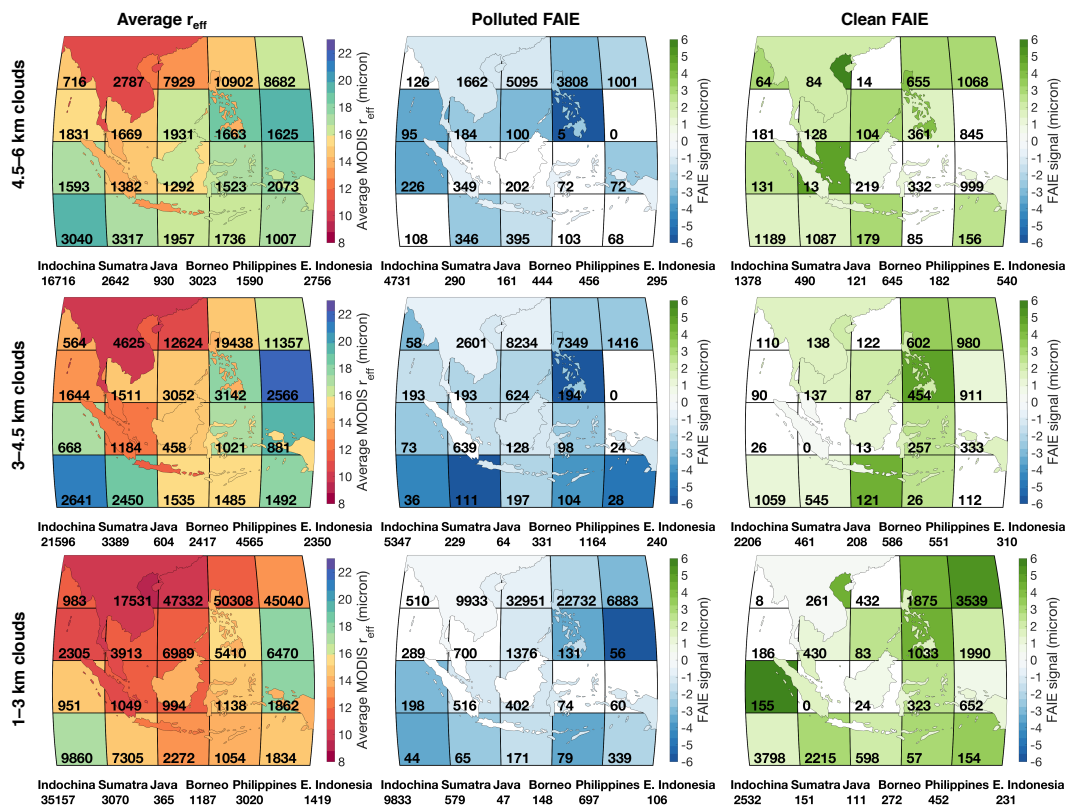
Figure 9: Identical to Fig. 8 but for winter months December through May.